# Light and Short Arc Rubs in Rotating Machines: Experimental Tests and Modelling

**P. Pennacchi, N. Bachschmid, E. Tanzi**
Politecnico di Milano, Department of Mechanical Engineering
Via La Masa 1, I-20156, Milan, Italy
paolo.pennacchi@polimi.it, nicolo.bachschmid@polimi.it, ezio.tanzi@mecc.polimi.it

## Abstract
Rotor-to–stator rub is a non-linear phenomenon which has been analyzed many times in rotordynamics literature, but very often these studies are devoted simply to highlight non-linearities, using very simple rotors, rather than to present reliable models. However, rotor-to-stator rub is actually one of the most common faults during the operation of rotating machinery. The frequency of its occurrence is increasing due to the trend of reducing the radial clearance between the seal and the rotor in modern turbine units, pumps and compressors in order to increase efficiency. Often the rub occurs between rotor and seals and the analysis of the phenomenon cannot set aside the consideration of the different relative stiffness. This paper presents some experimental results obtained by means of a test rig in which rub conditions of real machines are reproduced. In particular short arc rubs are considered and the shaft is stiffer than the obstacle. Then a model, suitable to be employed for real rotating machinery, is presented and the simulations obtained are compared with the experimental results. The model is able to reproduce the behaviour of the test rig.

## 1 Introduction

Rotor to stator rub in industrial rotating machinery can occur in different sections of the machine and can have different degrees of severity. In this paper, the interest is focused on rub that occurs between parts that have different stiffness, in particular when the rotor is stiffer than the stator or, more precisely, than the parts where the contact happens. This fact, which can appear unrealistic when thinking about massive casings, is on the contrary very frequent, when a working fluid is present. In order to increase machine efficiency, there is a trend to reduce the gap between the rotor and the fluid seals. Considering that rotating machinery can cross some critical speeds during the run-ups and the run-downs, the rotor can interfere with the seals in case of incorrect design, excessive imbalance, misalignment, bad assembly or other causes. Due to their specific function, these seals are often of labyrinth type and in this case the stiffness of the threads is less than that of the rotor. Figure 1 shows the effect of rub on a seal: threads are practically destroyed and the functionality of the seal is heavily damaged.

Several experimental cases have been documented in literature about rub occurred during operation or commissioning of real rotating machinery. Some of them are related to rub diagnostics and employ model based fault identification applied to vibration measurements, see [1][2][3]. Curami et al. [4] present the experimental evidence of a heavy rub in a 320 MW steam turbine and analyse the possible parametric instability due to the periodic radial stiffness variation of the rotor, concluding that this phenomenon is unlikely in real machines.

Stegemann et al. [5] describe long lasting tests on a 100 MW steam turbine with about 500 cases of rub, investigated by means of the combined use of vibration and acoustic emission. Hall and Mba [6] present a successful case of rub diagnosis on a 500 MW steam turbine using acoustic emission. These last studies highlight the presence of high frequency components in the measured noise.

Intense research activity has been also performed on test rigs. Due to the relative small scale of the rigs employed, rotor-to-stator rub phenomenon can be studied with more accuracy and in the controlled

environment of the laboratory. However, in some cases, test rigs are so small and simple, with very flexible shafts that can hardly reproduce the behaviour of real rotating machinery. Hall and Mba [7] have tuned up their method using a test rig in which partial rub is reproduced between a multi-disk rotor and several types of steel and brass fixture, reproducing seals. Anyhow the contact occurs as a consequence of the non-circular section of the shaft in correspondence of the seal, rather than of the rotor whirling.

**Figure 1: Effect of the rub on a labyrinth seal.**

Several experimental tests are also documented by Chu et al. [8][9][10][11] for a rather small test rig. Starting from the experimental observation that the so-called transient natural frequencies change once the rub-impact occurs, they analyse the increase of the transient stiffness of the rotor as the consequence of the interaction with the obstacle. The transient stiffness increasing is used to locate the position of the rub [8] and some test, aimed to identify it, are presented in [11], indicating that transient stiffness keeps on increasing with the rub–impact and aggravating when the speed is increasing. The study of the stiffness increasing is also presented by Fumagalli and Schweitzer [12] by means of a test rig, in which magnetic bearings are used as both exciters and sensors and the obstacle is rather stiff. The results obtained are similar to those of [11], even if the concept of transient stiffness is not introduced. Magnetic bearings are also used to prevent physical interaction between rotor and stator laminations by Keogh and Cole [13][14].

Keeping in mind the aspects related to the contact, Choy [15] discuss the combined effect of the rotor dynamical behaviour (i.e. rotor whirling) and of the relative speed between the rotor and the obstacle on the friction coefficient. From these results, it appears that the friction coefficient varies considerably from reference values when the rotating speed is close to the critical speed of the small test rig employed in the experiments. Other studies of the same author are focused on partial rub during speed transients, with the analysis of the rotor forward and backward whirling [16][17]. Experimental tests on partial arc rub are presented and discussed by Muszyńska [18][19], which observed that frequency behaviour patterns of the rotor response were systematically repeatable, but the specific orbits appeared quite unstable, especially when the rotor-to-stator normal forces are higher (i.e. when the interference between the rotor and the obstacle is higher) and the contact lasted longer. Authors share the explanation given to this: friction-related surface wear causes continual changes in clearance. Anyhow a deeper analysis is cumbersome: in case of real machinery, seals are relatively less stiff than the rotor and this cause not only wear but also seal plastic deformation. Consequently the transient stiffness varies sensibly. This notwithstanding plastic deformation is reduced in case of light rub and can be considered as a second order effect. The possibility to forecast the experimental chaotic motion of a test rig using a fitting technique is presented by Hu and Wen [20].

The precession and the effects of the friction force, especially with regard to dry-friction whirl and whip, are also analyzed repeatedly by Childs [21][22][23]. Bently et al. study the same problem, focusing on mechanical seals and on full-annular rub: experimental results obtained by using a small test rig are presented [24] and a mathematical model aimed to study the stability, but not to reconstruct experimental results, is introduced [25]. Stability analysis is the topic of several papers in literature: Jiang and Ulbrich [26][27] use a Jeffcott rotor model to perform the stability analysis of the full annular rub. A similar topic is studied by Muszyńska [28]. Also Ehehalt and Markert [29][30][31] study the stability thresholds by means of a Jeffcott rotor. Cole and Keogh [32] use a Jeffcott rotor model to analyse the stability of the rotor-to-stator contact of a test rig. Anyhow stability thresholds show that the interference should be so severe that rarely can occur in real machines without a catastrophic result and all these results appear not verified by experimental studies like [4]. Thus this paper is not focused on so severe rub and considers only short arc rubs.

Obviously, the presence of friction can cause also thermal effects during rub, but this aspect is not relevant in the case considered in the paper. Readers potentially interested on this topic can refer to [33], also for a pertinent literature survey.

Another interesting effect on the rotor dynamics, caused by rub, is the excitation of torsional vibrations. These vibrations can be considered as always present, but they are seldom measured, because real machineries are normally not equipped by a suitable device to measure them. The effect of rub on torsional vibration of the rotor is studied by Edwards et al. [34], by Huang [35] who presents an experimental study on the coupling of torsional and lateral vibrations and by Deng et al. [36] who uses a simplified Jeffcott rotor model to study the effect of the friction coefficient on the FFT full spectrum of the torsional vibration.

Many studies present in literature, apart from their remarkable scientific interest, consider only very simple rotordynamic systems and often they are more focused on the numerical simulation of non-linearities than on the dynamical behaviour of real rotating machinery. For instance, many papers consider Jeffcott/de Laval rotors, because they have few degrees of freedom (d.o.f.s) and the equations of motion can be written explicitly. In other cases, the stiffness of the seals and their d.o.f.s are neglected. However this kind of model for the rotor is not suitable to reproduce the behaviour of real machines, even though it is claimed that this represents a modal model of the rotor. The effectiveness of a modal approach in presence of non-linearities is rather questionable. These papers are often more concerned to show application of the theory of non-linear systems.

The aim of this paper is the study of short arc rub typical of light contact on seals. Since it is not realistic to study the rub between rotor and stator (in which a seal is installed) on-field, specific tests are performed on a test rig that is characterized by the most common features of real rotating machinery. Then a model has been set-up in order to reproduce the experimental results. Model employs standard rotordynamic methods, i.e. finite element for the shaft, dynamic stiffness coefficients for the bearings, and considers the effects of the supporting structure; therefore it can be applied to any type of rotating machine. Once the model is verified, the behaviour of real machines can be simulated as a consequence of rub, at least in the frequency range that is typical of the standard condition monitoring systems installed on rotating machineries. The validity of the model is restricted to a range of parameters characterizing light rubs and “soft” seals.

## 2 Description of the experimental set-up

The experimental tests of short arc rub were performed on the modular test rig of Politecnico di Milano. This test rig has been employed for several researches in the field of rotordynamics and its complete structure was fully described in [37]. One advantage of this test rig consists in its modularity and the configuration described in detail afterwards was adopted for the present research. In this configuration, only two bearings among the original four have been retained and the shaft is not overhung. The aim of this arrangement is to reproduce the behaviour of a section of horizontal industrial machines.

The general layout of the shaft is not symmetric and the rotor is not comparable at all to a Jeffcott/de Laval rotor. Figure 2 shows a picture of the test rig. The relative position of the inertia disks and the place

where the contact occur is aimed to reproduce that of seals on the ends of the bladed stages of turbomachinery.

The test rig is composed of a horizontal flexible shaft of 1485 mm length with a minimum diameter of 25 mm as shown in figure 2. The shaft is connected to an electrical motor, driven by inverter, by means of a flexible coupling and is carrying two disks of a diameter of 160 mm and a thickness of 110 mm. The total weight of the shaft is nearly 500 N. The motor drives the shaft from 0 up to a maximum speed of 6000 rpm, but tests are generally carried out at lower speeds, because the aim is to analyze the behaviour under and over the first critical speed.

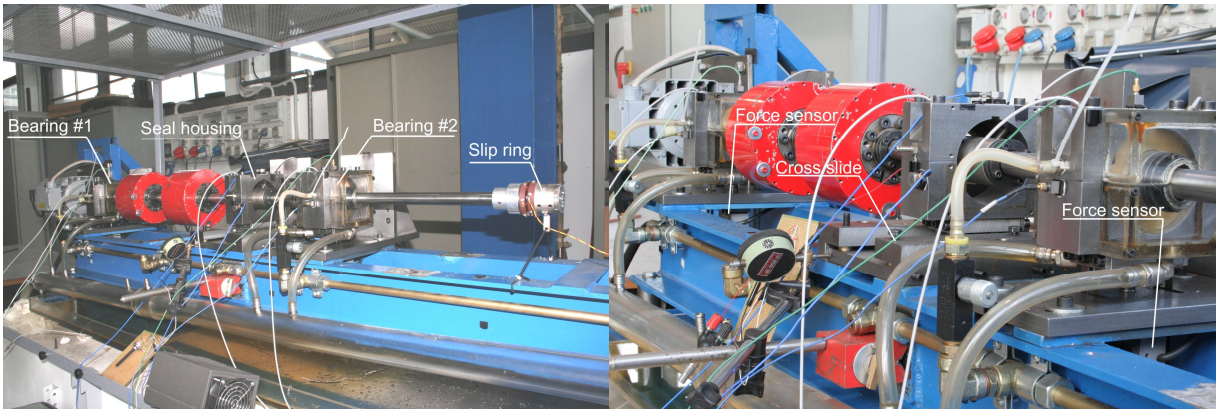


**Figure 2: Rotordynamic test rig of Politecnico di Milano.**

The shaft is supported by two lemon shaped oil-film bearings and by two bearing housings, connected to an oil circulation system to lubricate the bearings. The shaft has a diameter of 50 mm in correspondence of the bearings. The bearing housings are connected by means of two force sensors, in horizontal and vertical direction, to a metallic supporting structure. This makes the entire supporting structure rather flexible. Some supporting structure resonances are within the operating speed range of the test rig. The entire apparatus is clamped to a massive concrete block isolated from the environment by rubber pads.

Each bearing is equipped with two proximity probes in directions + and – 45° with respect to the vertical direction, as it is usual in many industrial machines. However, the signals from proximity probes are rotated after the acquisition, making the axis of the shaft displacement coincident with the horizontal and vertical directions, this procedure allows to compare all signals in vertical and horizontal directions.

The bearing housings are equipped with two accelerometers for measuring its vibrations in vertical and horizontal direction. A third housing is mounted on a cross slide, as shown in figure 3, between the second inertia disk and the bearing at the non-driven end (NDE), and can be moved in radial horizontal direction. A half seal strip is mounted on this support instead of the bearing, see figure 4.

The stiffness of this seal strip is less than that of the shaft in order to reproduce what happens in real machines, in which the contact occurs between the shaft and labyrinth seals. The cross slide allows the seal to be put in contact with the rotating shaft and to set the value of the interference; the diameter of the shaft has been enlarged to 50 mm and the seal strip has a diameter of 55 mm. The normal contact force is mainly horizontal and the tangential force vertical, due to the geometry of the contact imposed by the slide. Also this support is equipped with proximity probes, with force sensors and with accelerometers.

Unfortunately, the upper limit of the frequency response of the force sensor is rather low with respect to the frequencies that could be excited and consequently force signal was not taken into account for these tests.

Finally also a contact sensor has been designed, tested and installed for measuring the duration of the contact. It is composed by Wheatstone's bridge with one node connected to the shaft, by means of a slip ring installed on the extreme end of the NDE of the rotor that is visible in figure 2, and the other connected to the seal strip that is the clip in figure 4. Due to the low voltage, the oil film in the bearings guarantees the electric isolation of the shaft from the base and the supports. After tuning, the voltmeter indicates 0 V

when no contact occurs, and indicates 2.5 V during contact. The upper limit of the frequency response of this sensor is greater than 10 kHz.

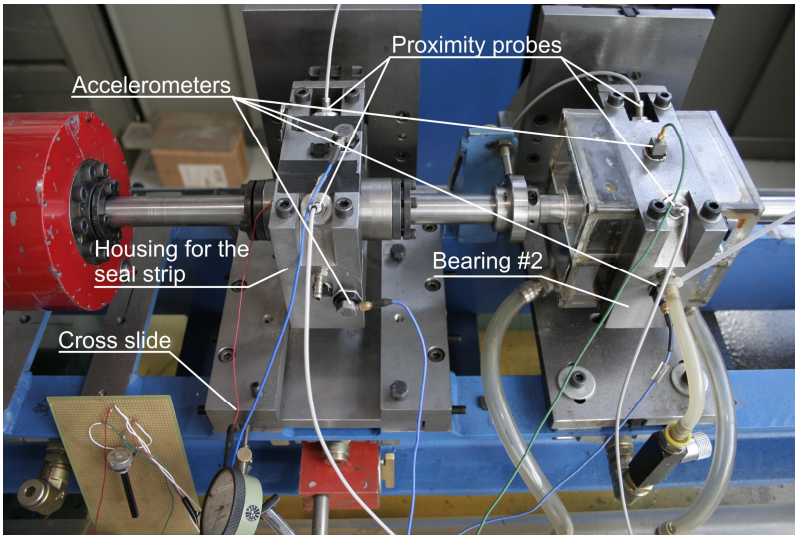


**Figure 3: Cross slide and housing in which the seal strip is installed.**

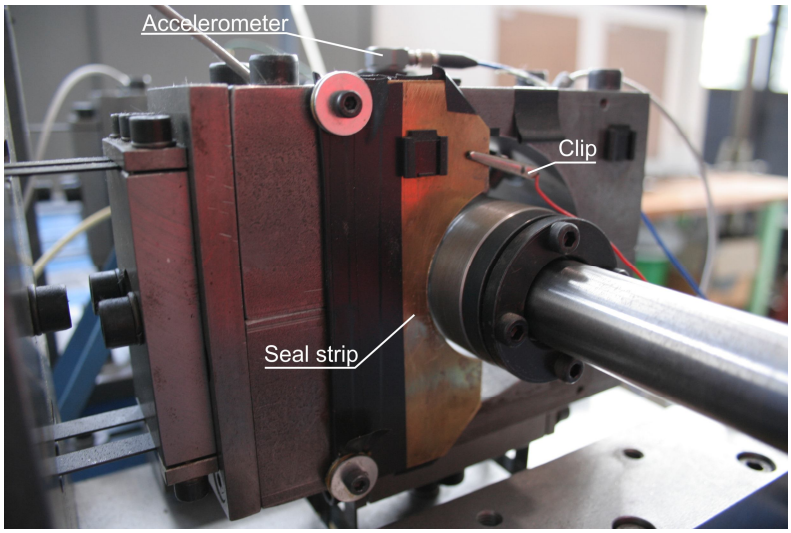


**Figure 4: Close-up of the seal strip and of the flexible structure that support the housing.**

The first critical speed of the rotor system is split in horizontal and vertical directions of about 30 rpm, but it is about 1050 rpm. In order to explore the behaviour of the system under and over the critical speed, the tests were performed at 600 and 1200 rpm.

From the experimental cases presented in literature [5][6], high frequency components of the vibration are excited by the rub and this motivate the possibility to detect the presence of a rub by means of acoustical measurements. A simple test was performed on the test rig by comparing the vibration of the seal support and the corresponding acoustic emission without and with severe rub, in order to confirm this possibility. Figure 5 shows the power spectral density of the vibrations of the seal ring support, measured by the accelerometer, and the associated noise emission, measured by a microphone placed at a distance of 0.5 m from the support at the rotating speed of 1200 rpm. The rub, being its nature mainly impulsive, increases consistently (up to two orders of magnitude) the vibration amplitudes in the complete range of frequency of the accelerometer (1 – 7000 Hz).

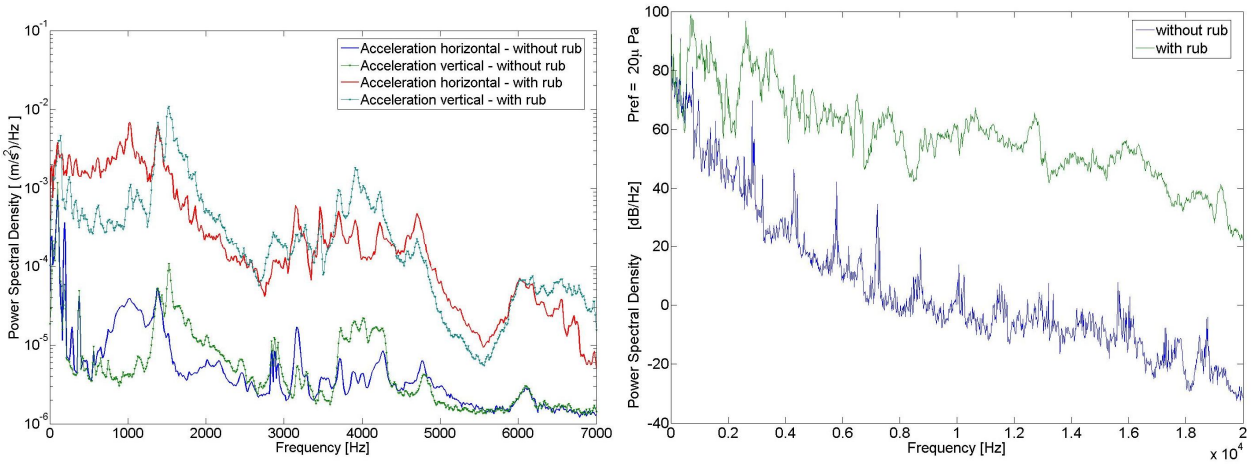


**Figure 5: Power spectral density of acceleration of support 3 (left) and of the sound pressure (right).**

Anyway, normally standard condition monitoring systems installed on real rotating machineries consider only low frequency vibrations and the challenging task is to detect the rub in its initial stage (not simply by "hearing it"). Therefore the experimental results here presented consider light rubs and low frequency range. More experimental results of heavy rub conditions are presented in [38]. Also the model developed in the second part of the paper will be used to simulate the dynamic behaviour in the low frequency range.

## 2.1 Experimental results obtained at 600 rpm

The tests at 600 rpm were performed by setting the rotating speed in the motor driver control, then running up the rotor at rated speed and then moving the slide until contact is reached. The presence of a comparator allows a rough evaluation of the interference between the seal strip and the rotor, because, as stressed in the introduction, friction-related surface wear causes continual changes in the clearance. The shape of the rotor orbits after rub strongly depends on the amount of the interference and in this study only light rubs are considered.

The experimental orbits in correspondence of the seal and of the bearings are plotted in figure 6-figure 8 for the duration of 1 s, when the interference is equal to 5 μm. The positions of the beginning and end of the contact are obtained by comparing the time histories of the vibrations and of the contact sensor. Anyhow it is interesting to observe that actually the contact is not continuous, as shown in figure 9 for one rotor revolution, thus the rotor and the seal rub each other intermittently. The time interval, in which contacts happen, lasts about a quarter of the period of revolution.

All the orbits in the measuring planes are distorted with respect to elliptical ones, included in the bearings, which are the planes where vibrations are normally measured in real machines. Besides other effects, rub tends to reduce orbit amplitude as it is shown in figure 7, where the orbit without rub is shown as a dashed line. Obviously the orbit without rub is pretty well elliptical due to the presence of the residual unbalance only and to the high degree of linearity of the system. This fact can be explained by keeping in mind the concept of the transient stiffness introduced in [8] [11]. The overall system becomes stiffer as a consequence of the rub, and being below the critical speed, the vibration amplitude is reduced at constant speed. A qualitative explanation is given in figure 10. Similar reductions of the orbits amplitude in presence of rub are obtained also in the seal position and in bearing #2 and are omitted from figure 8 for clarity.

Finally, if the vibration spectra in the measuring planes are considered, see figure 11 to figure 13 in which the orders up to 10× are displayed, it is rather evident to observe the presence of the major synchronous component and of the super-harmonics of integer-order, that indicate the non-linear characteristic of rubbing. Anyhow, the super-harmonic components are rather small due to light rub, especially in the bearings (note that a logarithmic scale has been used for the amplitudes).

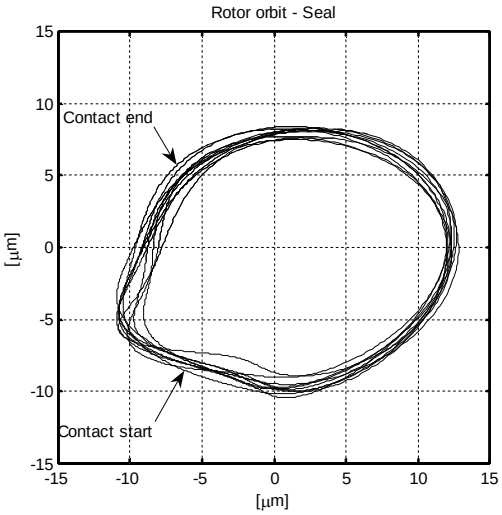


**Figure 6: Rotor orbit in seal position at 600 rpm.**

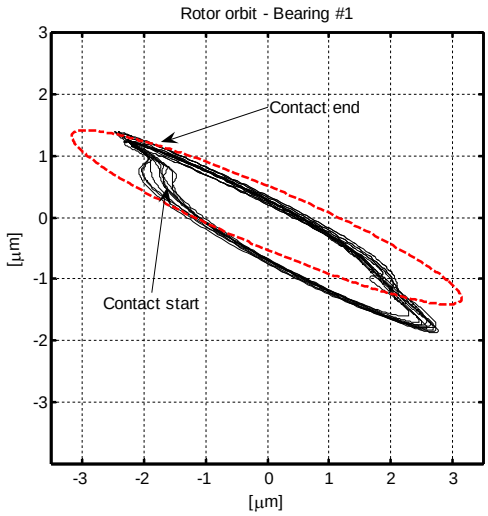


**Figure 7: Rotor orbit in bearing #1 at 600 rpm.**

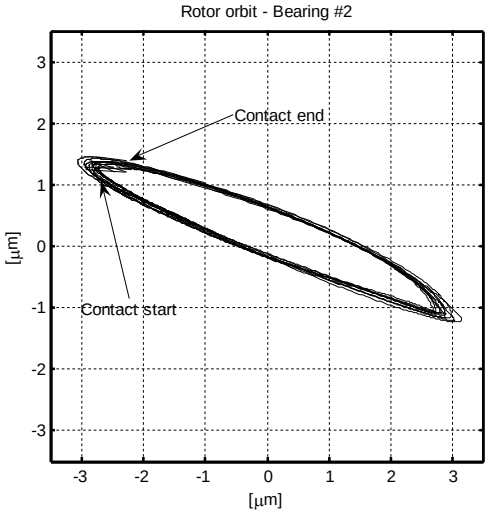


**Figure 8: Rotor orbit in bearing #2 at 600 rpm.**

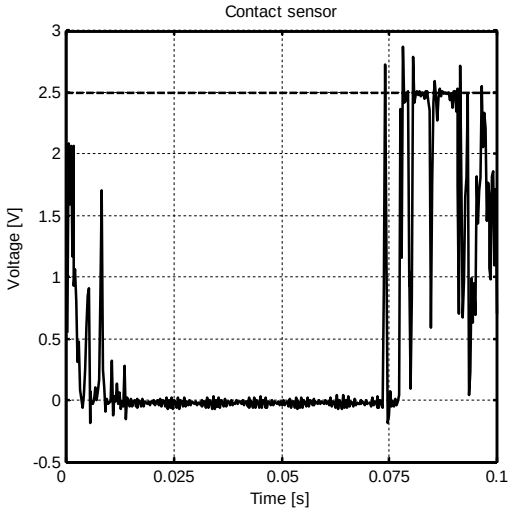


**Figure 9: Time history of the contact signal over one revolution.**

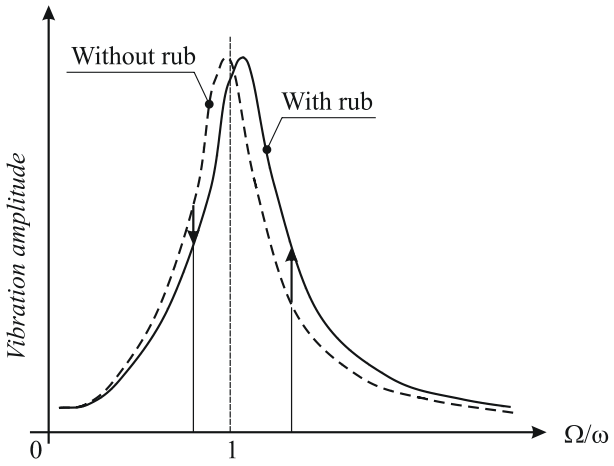


**Figure 10: Qualitative explanation of orbit size change caused by transient stiffness.**

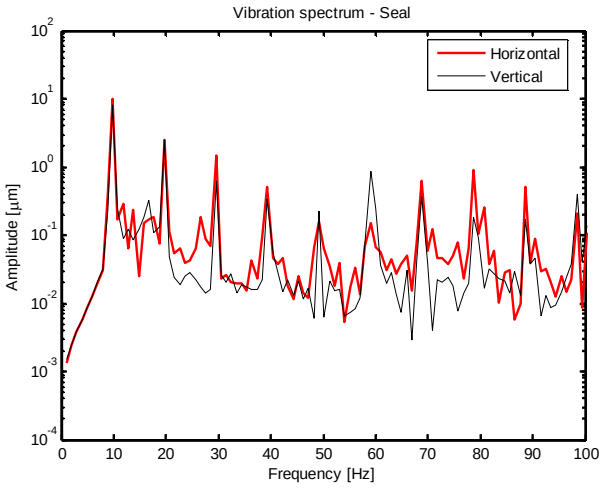


**Figure 11: Vibration spectrum in seal position at 600 rpm.**

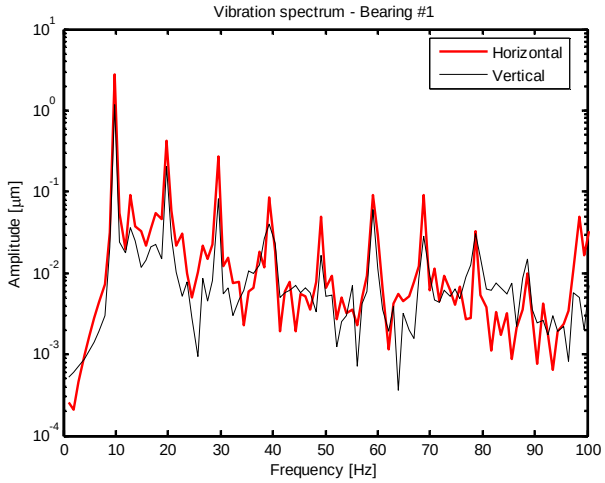


**Figure 12: Vibration spectrum in bearing #1 at 600 rpm.**

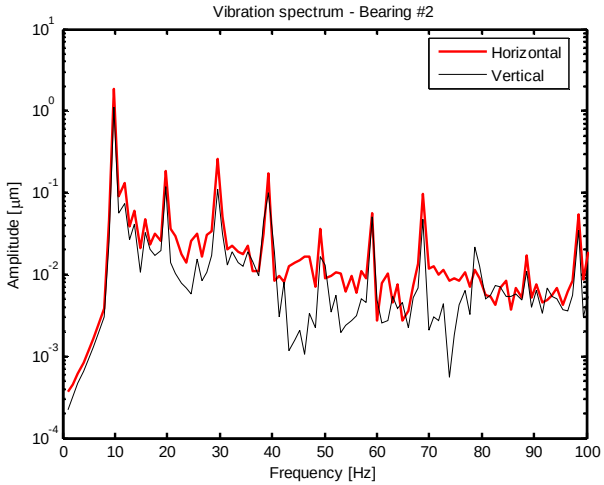


**Figure 13: Vibration spectrum in bearing #2 at 600 rpm.**

## 2.2 Experimental results obtained at 1200 rpm

The tests performed at 1200 rpm, over the first critical speed, followed the same procedure of those at 600 rpm. Also in this case the rub is intentionally light and the orbits are shown in figure 14-figure 16. Rotor orbit in the seal position, see figure 14, is rather deformed in the part where the contact occurs, while the orbits in the bearings present some perturbation also on the opposite part. Similarly to the previous case, the contact between the rotor and the seal is intermittent, see figure 17, and the time interval is less than a quarter of the period of revolution.

Contrary to the previous case, orbit amplitude during the rub is “inflated” with respect to the non-rubbing condition, as can be observed in figure 15, where the orbit before rub is shown in dashed line. Also this phenomenon can be explained by the transient stiffness, considering that the system is operating over the

first critical speed (see figure 10). Similar results are obtained also in the seal position and bearing #2 and the orbits before rub are omitted from figure 16 for clarity.

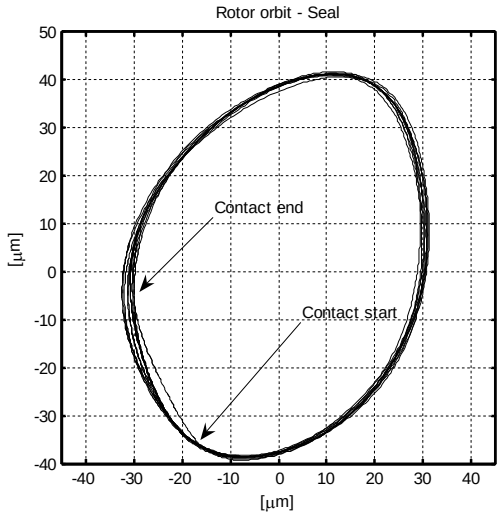


**Figure 14: Rotor orbit in seal position at 1200 rpm.**

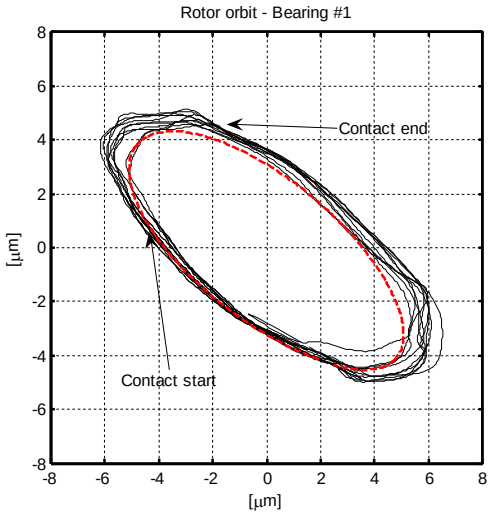


**Figure 15: Rotor orbit in bearing #1 at 1200 rpm.**

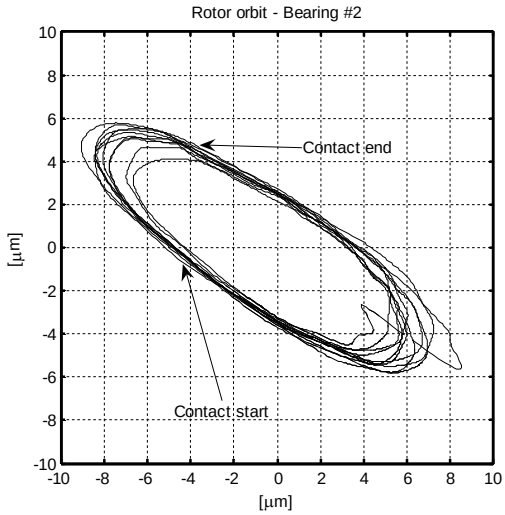


**Figure 16: Rotor orbit in bearing #2 at 1200 rpm.**

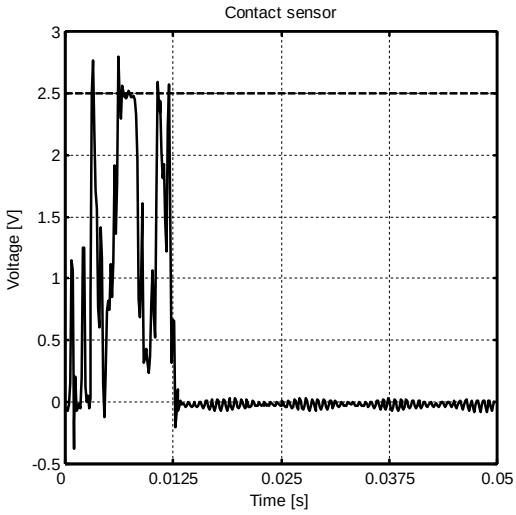


**Figure 17: Time history of the contact signal over one revolution.**

Vibration spectra, shown in figure 18-figure 20 up to the 10× order, highlight the highest component of the synchronous vibration and several integer-order super-harmonics. These last are caused by the intrinsic non-linear characteristics of the rub.

## 3 Model description

The complete model of the system is described in this section, even if some simplification about the supporting structure will be actually introduced in the following. The aim of the model is to simulate not only the behaviour of the test rig, but also that of real machines. Thus, the rotor is modelled by means of finite beam elements, taking also into account the gyroscopic, the shear and the secondary effect of rotatory inertia.

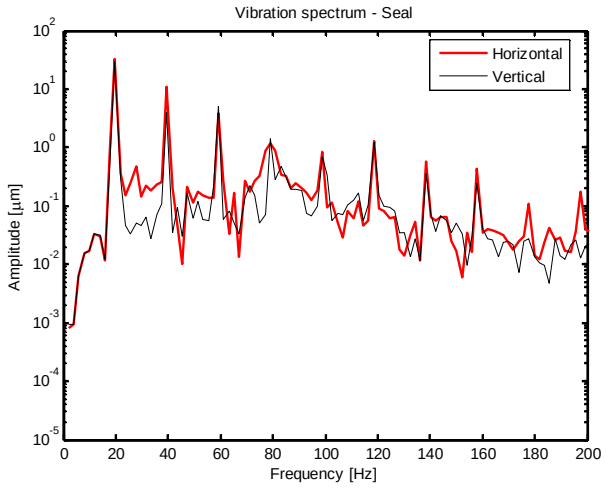


**Figure 18: Vibration spectrum in seal position at 1200 rpm.**

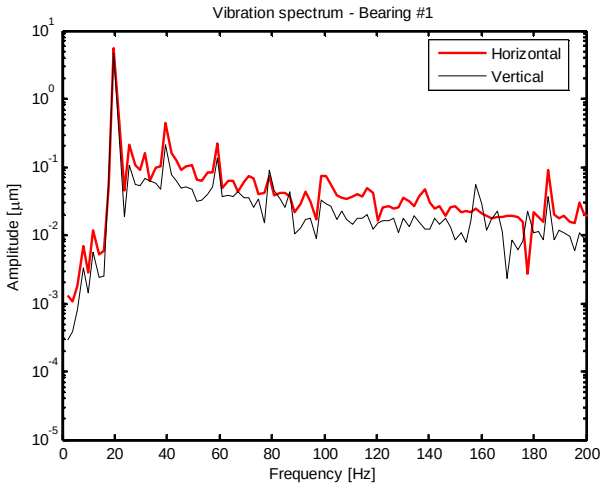


**Figure 19: Vibration spectrum in bearing #1 at 1200 rpm.**

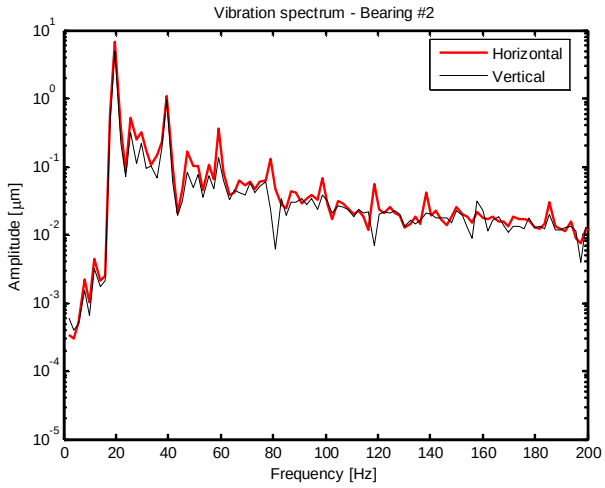


**Figure 20: Vibration spectrum in bearing #2 at 1200 rpm.**

Even if the experimental tests of paper deal only with the lateral response, the model is set up in order to consider also the torsional vibration and 5 degrees of freedom (d.o.f.s) - two translational and three rotational - are considered per each node. On the contrary, axial vibrations will be neglected. Considering the general *j*-th element of the rotor, the generalized displacement vector $\mathbf{x}_j^{(r)}$ of the rotor *j*-th node is ordered as follows:

$$\mathbf{x}_j^{(r)} = \left\{ x_j^{(r)} \quad y_j^{(r)} \quad \vartheta_{x_j}^{(r)} \quad \vartheta_{y_j}^{(r)} \quad \vartheta_{z_j}^{(r)} \right\}^{\mathrm{T}} \tag{1}$$

Two subsequent nodes, the *j*-th and the *j*+1-th, define the *j*-th element of the machine. If the rotor has $n_r$ nodes, thus $n_r - 1$ elements, the vector $\mathbf{x}^{(r)}$ of the generalized displacements of all the rotor nodes is composed by all the ordered vectors $\mathbf{x}_j^{(r)}$ as shown in eq. (2):

$$\mathbf{x}^{(r)} = \left\{ x_1^{(r)} \quad y_1^{(r)} \quad \vartheta_{x_1}^{(r)} \quad \vartheta_{y_1}^{(r)} \quad \vartheta_{z_1}^{(r)} \cdots x_{n_r}^{(r)} \quad y_{n_r}^{(r)} \quad \vartheta_{x_{n_r}}^{(r)} \quad \vartheta_{y_{n_r}}^{(r)} \quad \vartheta_{z_{n_r}}^{(r)} \right\}^{\mathrm{T}} \tag{2}$$

Different methods can be used to model the foundation. For the sake of brevity, only pedestals, i.e. lumped 2 d.o.f.s systems, will be considered. A discussion about other methods is reported in [39]. In a similar manner to the rotor, also the d.o.f.s of the foundation, horizontal and vertical displacements, which are connected by the $n_b$ bearings to the rotor, can be ordered in a vector:

$$\mathbf{x}^{(f)} = \left\{ x_1^{(f)} \quad y_1^{(f)} \cdots x_{n_b}^{(f)} \quad y_{n_b}^{(f)} \right\}^{\mathrm{T}} \tag{3}$$

Finally, the seal strip and its housing will be considered as the rigid body P, connected to the reference by means of lumped stiffness and damping parameters (see figure 21), that has 6 d.o.f.s:

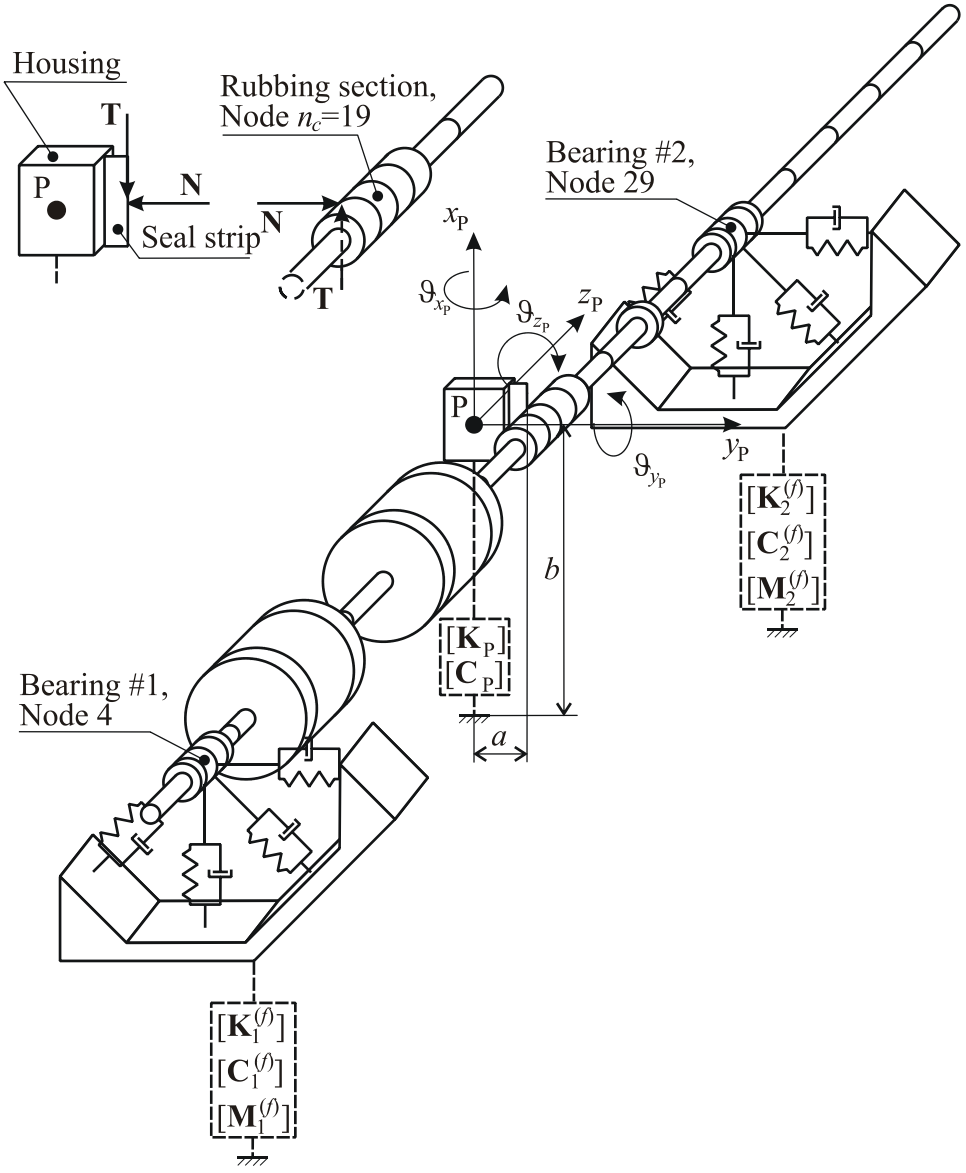


**Figure 21: Model of the test rig.**

$$\mathbf{x}_P = \left\{ x_P \quad y_P \quad z_P \quad \vartheta_{x_P} \quad \vartheta_{y_P} \quad \vartheta_{z_P} \right\}^{\mathrm{T}} \tag{4}$$

The corresponding node on the rotor, where the contact with the seal occurs, is indicated as node $n_c$ and it is #19 in the finite beam model of the considered test rig.

The complete vector of the generalized displacements of the system is therefore:

$$\mathbf{x} = \left\{ \mathbf{x}^{(r)} \quad \mathbf{x}^{(f)} \quad \mathbf{x}_{\mathrm{P}} \right\}^{\mathrm{T}} \tag{5}$$

With regard to the rotor, the mass matrix $[\mathbf{M}^{(r)}]$, which takes also into account the secondary effect of the rotatory inertia, the internal damping matrix $[\mathbf{C}^{(r)}]$, the stiffness matrix $[\mathbf{K}^{(r)}]$, which takes also into account the shear effect, and the gyroscopic matrix $[\mathbf{G}^{(r)}]$, all of order $(5n_r \times 5n_r)$, can be defined by means of standard Lagrange's methods, beam elements and lumped disks as shown e.g. in [22][40]. Whilst the structure of $[\mathbf{M}^{(f)}]$, $[\mathbf{C}^{(f)}]$ and $[\mathbf{K}^{(f)}]$ is not relevant at this stage and depends on how the supporting structure is implemented, the matrices of the seal housing are all simply diagonal matrices:

$$[\mathbf{M}_{\mathrm{P}}] = \mathrm{diag}(m_{\mathrm{P}}, m_{\mathrm{P}}, m_{\mathrm{P}}, I_{\mathrm{P}_x}, I_{\mathrm{P}_y}, I_{\mathrm{P}_z}) \tag{6}$$

$$[\mathbf{C}_{\mathrm{P}}] = \mathrm{diag}(c_{\mathrm{P}_x}, c_{\mathrm{P}_y}, c_{\mathrm{P}_z}, c_{t\mathrm{P}_x}, c_{t\mathrm{P}_y}, c_{t\mathrm{P}_z}) \tag{7}$$

$$[\mathbf{K}_{\mathrm{P}}] = \mathrm{diag}(k_{\mathrm{P}_x}, k_{\mathrm{P}_y}, k_{\mathrm{P}_z}, k_{t\mathrm{P}_x}, k_{t\mathrm{P}_y}, k_{t\mathrm{P}_z}) \tag{8}$$

Obviously the evaluation of these parameters is rather difficult considering a real machine. In the case of the test rig, the estimation can be done experimentally, for instance by means of modal analysis. Anyhow, some of the values of inertia and stiffness parameters employed for the simulations have been obtained by means of impact test, some other have been assigned on the basis of their likelihood to reproduce the approach of a real machine and the values are reported in table 1. As shown in paragraphs 3.1 and 3.2, these values allow a good fitting with the experimental tests.

**Table 1: Seal strip housing parameters used for the simulation.**

| | | | | | |
|---|---|---|---|---|---|
| $m_{\mathrm{P}}$ | 10 kg | $c_{\mathrm{P}_x}$ | 1000 Ns/m | $k_{\mathrm{P}_x}$ | 2.5e6 N/m |
| $I_{\mathrm{P}_x}$ | 0.1 kgm$^2$ | $c_{\mathrm{P}_y}$ | 1000 Ns/m | $k_{\mathrm{P}_y}$ | 2e6 N/m |
| $I_{\mathrm{P}_y}$ | 0.2 kgm$^2$ | $c_{\mathrm{P}_z}$ | 2000 Ns/m | $k_{\mathrm{P}_z}$ | 3e5 N/m |
| $I_{\mathrm{P}_z}$ | 0.3 kgm$^2$ | $c_{t\mathrm{P}_x}$ | 10 Nm s | $k_{t\mathrm{P}_x}$ | 2e4 Nm |
| | | $c_{t\mathrm{P}_y}$ | 10 Nm s | $k_{t\mathrm{P}_y}$ | 2e4 Nm |
| | | $c_{t\mathrm{P}_z}$ | 10 Nm s | $k_{t\mathrm{P}_z}$ | 2e4 Nm |

The test rig rotor is supported by $n_b$ oil-film bearings that realize a coupling between the rotor and the supporting structure. Even if the exact calculation of the forces exchanged between the journal and the bearing case, due to the oil-film, requires appropriate methods, the discussion of which is far from the scope of present paper, a widely accepted simplification in rotor-dynamics simulation (see again [40]) is the modelling of the oil-film force field by means of linearized stiffness and damping coefficients as a function of the rotating speed. Therefore, the expression of the linearized forces of the oil-film of the *i*-th bearing on the rotor journal located in the *j*-th node, due to the rotor d.o.f. displacements only, is:

$$\mathbf{F}_i^{(br)}(\Omega) = -\begin{bmatrix} k_{xx_i}^{(b)}(\Omega) & k_{xy_i}^{(b)}(\Omega) & 0 & 0 & 0 \\ k_{yx_i}^{(b)}(\Omega) & k_{yy_i}^{(b)}(\Omega) & 0 & 0 & 0 \\ 0 & 0 & 0 & 0 & 0 \\ 0 & 0 & 0 & 0 & 0 \\ 0 & 0 & 0 & 0 & 0 \end{bmatrix} \begin{Bmatrix} x_j^{(r)} \\ y_j^{(r)} \\ \vartheta_{x_j}^{(r)} \\ \vartheta_{y_j}^{(r)} \\ \vartheta_{z_j}^{(r)} \end{Bmatrix} - \begin{bmatrix} c_{xx_i}^{(b)}(\Omega) & c_{xy_i}^{(b)}(\Omega) & 0 & 0 & 0 \\ c_{yx_i}^{(b)}(\Omega) & c_{yy_i}^{(b)}(\Omega) & 0 & 0 & 0 \\ 0 & 0 & 0 & 0 & 0 \\ 0 & 0 & 0 & 0 & 0 \\ 0 & 0 & 0 & 0 & 0 \end{bmatrix} \begin{Bmatrix} \dot{x}_j^{(r)} \\ \dot{y}_j^{(r)} \\ \dot{\vartheta}_{x_j}^{(r)} \\ \dot{\vartheta}_{y_j}^{(r)} \\ \dot{\vartheta}_{z_j}^{(r)} \end{Bmatrix} = \tag{9}$$

$$= -\left[\mathbf{K}_i^{(b)}(\Omega)\right]\mathbf{x}_j^{(r)} - \left[\mathbf{C}_i^{(b)}(\Omega)\right]\dot{\mathbf{x}}_j^{(r)}$$

while that of the forces on the supporting structure, modelled by means of pedestals, corresponding to the *i*-th bearing and due to the foundation d.o.f. only, is:

$$\begin{aligned}\mathbf{F}_i^{(bf)}(\Omega) &= -\begin{bmatrix} k_{xx_i}^{(b)}(\Omega) & k_{xy_i}^{(b)}(\Omega) \\ k_{yx_i}^{(b)}(\Omega) & k_{yy_i}^{(b)}(\Omega) \end{bmatrix}\begin{Bmatrix} x_j^{(f)} \\ y_j^{(f)} \end{Bmatrix} - \begin{bmatrix} c_{xx_i}^{(b)}(\Omega) & c_{xy_i}^{(b)}(\Omega) \\ c_{yx_i}^{(b)}(\Omega) & c_{yy_i}^{(b)}(\Omega) \end{bmatrix}\begin{Bmatrix} \dot{x}_j^{(f)} \\ \dot{y}_j^{(f)} \end{Bmatrix} = \\ &= -\left[\widehat{\mathbf{K}}_i^{(b)}(\Omega)\right]\mathbf{x}_j^{(f)} - \left[\widehat{\mathbf{C}}_i^{(b)}(\Omega)\right]\dot{\mathbf{x}}_j^{(f)}\end{aligned} \tag{10}$$

The actual bearing force between the rotor and the foundation is given by the difference between eq. (9) and eq. (10). This way the coupling effect of the oil-film forces is taken into account by the relative displacements of the nodes of the rotor and of the foundation in correspondence of the bearings and the fully assembled system of equation is built up.

This requires the definition of the stiffness coupling matrices $[\mathbf{K}^{(rr)}]$, $[\mathbf{K}^{(rf)}]$, $[\mathbf{K}^{(fr)}]$, $[\mathbf{K}^{(ff)}]$ and the corresponding damping matrices $[\mathbf{C}^{(rr)}]$, $[\mathbf{C}^{(rf)}]$, $[\mathbf{C}^{(fr)}]$, $[\mathbf{C}^{(ff)}]$, which are sparse and respectively of order $(5n_r \times 5n_r)$, $(5n_r \times 2n_b)$, $(2n_b \times 5n_r)$ and $(2n_b \times 2n_b)$. The structure for the stiffness matrices is:

$$[\mathbf{K}^{(rr)}] = \mathrm{diag}\left(\cdots \quad \left[\mathbf{K}_i^{(b)}(\Omega)\right] \quad \cdots\right) \tag{11}$$

$$[\mathbf{K}^{(fr)}] = \begin{bmatrix} \cdots & \cdots & \cdots & \cdots & \cdots & \cdots & \cdots \\ \cdots & k_{xx_i}^{(b)}(\Omega) & k_{xy_i}^{(b)}(\Omega) & 0 & 0 & 0 & \cdots \\ \cdots & k_{yx_i}^{(b)}(\Omega) & k_{yy_i}^{(b)}(\Omega) & 0 & 0 & 0 & \cdots \\ \cdots & \cdots & \cdots & \cdots & \cdots & \cdots & \cdots \end{bmatrix} \tag{12}$$

$$[\mathbf{K}^{(rf)}] = \begin{bmatrix} \cdots & \cdots & \cdots & \cdots \\ \cdots & k_{xx_i}^{(b)}(\Omega) & k_{xy_i}^{(b)}(\Omega) & \cdots \\ \cdots & k_{yx_i}^{(b)}(\Omega) & k_{yy_i}^{(b)}(\Omega) & \cdots \\ \cdots & 0 & 0 & \cdots \\ \cdots & 0 & 0 & \cdots \\ \cdots & 0 & 0 & \cdots \\ \cdots & \cdots & \cdots & \cdots \end{bmatrix} \tag{13}$$

$$[\mathbf{K}^{(ff)}] = \mathrm{diag}\left(\cdots \quad \left[\widehat{\mathbf{K}}_i^{(b)}(\Omega)\right] \quad \cdots\right) \tag{14}$$

Damping matrices have similar structure, while the dependence of $\Omega$ is omitted hereafter for the sake of brevity. This way, the fully assembled system of equations, without excitation, results:

$$\left[\mathbf{M}\right]\ddot{\mathbf{x}} + \left[\mathbf{C}\right]\dot{\mathbf{x}} + \left[\mathbf{K}\right]\mathbf{x} = 0 \tag{15}$$

with:

$$[\mathbf{M}] = \begin{bmatrix} [\mathbf{M}^{(r)}] & \mathbf{0} & \mathbf{0} \\ \mathbf{0} & [\mathbf{M}^{(f)}] & \mathbf{0} \\ \mathbf{0} & \mathbf{0} & [\mathbf{M}_{\mathrm{P}}] \end{bmatrix} \tag{16}$$

$$[\mathbf{C}] = \begin{bmatrix} [\mathbf{C}^{(r)}] + \Omega[\mathbf{G}^{(r)}] + [\mathbf{C}^{(rr)}] & -[\mathbf{C}^{(rf)}] & \mathbf{0} \\ -[\mathbf{C}^{(fr)}] & [\mathbf{C}^{(f)}] + [\mathbf{C}^{(ff)}] & \mathbf{0} \\ \mathbf{0} & \mathbf{0} & \left[\mathbf{C}_{\mathrm{P}}\right] \end{bmatrix} \tag{17}$$

$$[\mathbf{K}]=\begin{bmatrix}[\mathbf{K}^{(r)}]+[\mathbf{K}^{(rr)}] & -[\mathbf{K}^{(rf)}] & \mathbf{0}\\ -[\mathbf{K}^{(fr)}] & [\mathbf{K}^{(f)}]+[\mathbf{K}^{(ff)}] & \mathbf{0}\\ \mathbf{0} & \mathbf{0} & [\mathbf{K}_{\mathrm{P}}]\end{bmatrix} \tag{18}$$

Due to the layout of the test rig in which the direction of the contact is mainly horizontal, the rub between the rotor and the seal strip occurs when the relative horizontal vibration between the node corresponding to the rub section and the housing exceeds the seal clearance $\delta$. This special geometry of the contact causes the $z_{\mathrm{P}}$, $\vartheta_{x_{\mathrm{P}}}$ and $\vartheta_{y_{\mathrm{P}}}$ directions to be not excited. Anyway they were considered in the model for completeness and for possibly dealing with other contact geometries. If this condition is verified, the equations of motion of the rotor+bearings+foundation and of the seal housing become coupled. Accordingly to other studies in literature presented in the introduction (e.g. [8][11][18][25][28][34]) and considering light rubs, the force system, exchanged between the rotor and the stator, is composed by:

- the normal component determined by the elastic reaction proportional to the penetration of the rotor in the sealing. The contact stiffness is assumed $k_c = 1e6$ N/m;
- the friction tangential reaction determined by Coloumb's law. Friction coefficient is assumed $\mu = 0.3$;
- the torques caused by the aforementioned forces on the rotor and on the housing.

In other terms:

if $\left(y_{n_c}(t)-y_{\mathrm{P}}(t)\right)>\delta$:

$$\mathbf{F}_c(\mathbf{x},t)=\left\{\cdots \underbrace{-\mu N \quad -N \quad 0 \quad 0 \quad -\mu N\frac{d_{m_{n_c}}}{2}}_{\text{node } n_c}\cdots \underbrace{\mu N \quad N \quad 0 \quad 0 \quad 0 \quad \mu Na+Nb}_{\text{housing}}\right\}^{\mathrm{T}}, \tag{19}$$

$$N=k_c\left(y_{n_c}(t)-y_{\mathrm{P}}(t)-\delta\right)$$

where $d_{m_{n_c}}$ is the external diameter of mass in correspondence of node $n_c$.

The friction torque acting on the rotor has the effect to decelerate the rotor. Anyhow, the actual test rig is driven by an electric motor that can hold a constant average rotating speed. Since the aim of the paper is not to accurately model the motor driving control (actually its parameters have not been identified), its effect on the rotor is simply modelled by means of a motor torque control. Moreover the results regarding torsional vibrations are not considered because they cannot be compared to experimental ones. Obviously the modelling of the motor control will allow using this model also to study torsional vibrations.

The remaining external forcing systems acting on the rotor are the weight $\mathbf{W}$ and the residual unavoidable unbalance distribution:

$$\mathbf{F}_{unb}(t)=\left\{\cdots \underbrace{me\Omega^2\cos\left(\Omega t+\varphi_{unb}\right) \quad me\Omega^2\sin\left(\Omega t+\varphi_{unb}\right) \quad 0 \quad 0 \quad 0\cdots}_{\text{node 15}}\right\}^{\mathrm{T}} \tag{20}$$

Note that the rotor unbalance has been identified using the method described in [37][39] for the considered layout of the test rig. The unbalance is in correspondence of the second inertia disk (node #15) and this result is used for the simulations presented in the following.

By considering all the excitations, the fully assembled system of equations is non-linear due to the rub effect and results:

$$[\mathbf{M}]\ddot{\mathbf{x}}+[\mathbf{C}]\dot{\mathbf{x}}+[\mathbf{K}]\mathbf{x}=\mathbf{F}_c(t)+\mathbf{M}(t)+\mathbf{F}_{unb}(t)+\mathbf{W}=\mathbf{F}(t)+\mathbf{W} \tag{21}$$

The non-linear system of equations in eq. (21) is integrated in the time domain using the Newmark's implicit method, in which the condition of eq. (19) is checked in each time step, in order to evaluate if rub happens.

### 3.1 Simulation results at 600 rpm

Contrary to the experimental cases in which only a rough evaluation of the interference between the rotor and the seal is possible, the proposed model allows it very accurately. Anyhow steps of roughly 5 µm were used to reproduce the accuracy in the positioning of the seal strip obtained in the experimental tests. Simulated orbits, shown in figure 22-figure 24 for 1 s, are compared in the same figures with the experimental ones at 600 rpm of figure 6 to figure 8. Orbits are reproduced very well, especially considering the size, the aspect ratio and position in which the contact starts and ends. Note that the reference system in the simulations is not the same of the experimental measurements, being that of the absolute vibration, the origin of which is in the centre of the bearings. In this case the effect of the weight and of the oil-film forces determine the position of the shaft centreline. Experimental orbits have been rigidly shifted.

Also the contact is not continuous, as shown in figure 25, where the time history over one revolution of a Boolean variable, equal to 1 when the condition in eq. (19) is true, is displayed. Note that in this case the beginning of the period is not coincident with that of figure 25. The model reproduces well the time interval of the contacts that occur in about one quarter of the revolution period. However, the contact is more intermittent and this indicates that the damping is somewhat underestimated in the model. This could be due to the fact that plastic energy dissipation is not considered.

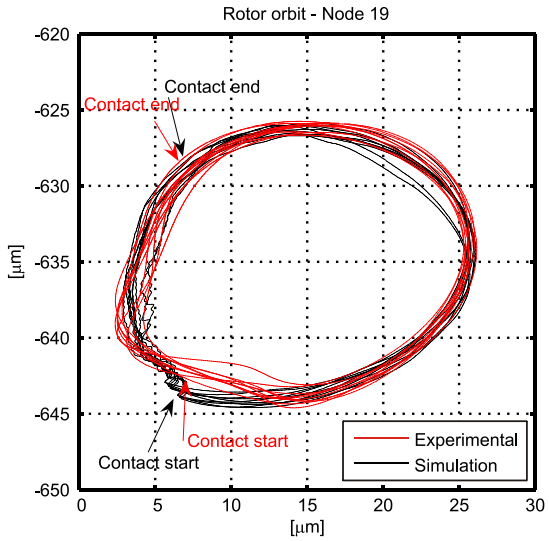


**Figure 22: Rotor orbit in seal position at 600 rpm.**

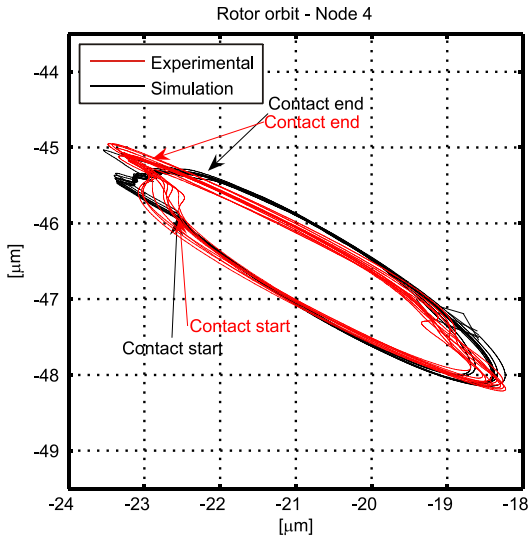


**Figure 23: Rotor orbit in bearing #1 at 600 rpm.**

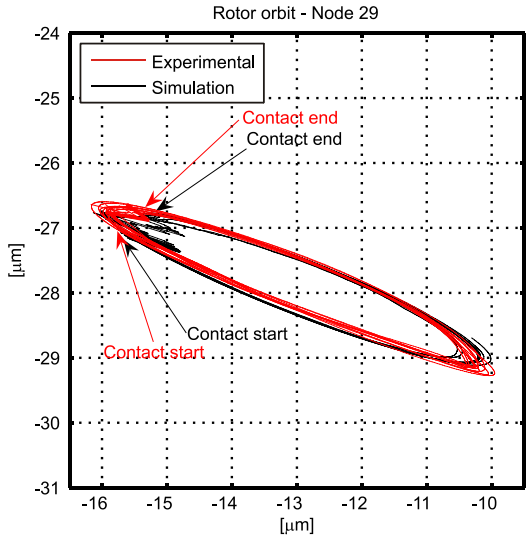


**Figure 24: Rotor orbit in bearing #2 at 600 rpm.**

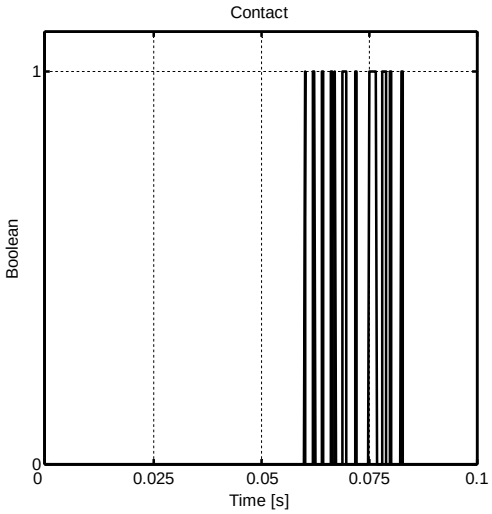


**Figure 25: Time history of the contact over one revolution.**

With regard to the vibration spectra, see figure 26 to figure 28, the presence of integer-order super-harmonics is evident and their amplitudes are comparable with those of the corresponding experimental case in figure 11-figure 13. However, in this case $n\times$ components are better pointed out due to the higher frequency resolution used in the numerical simulation. The amplitudes of the harmonics are comparable to the experimental ones.

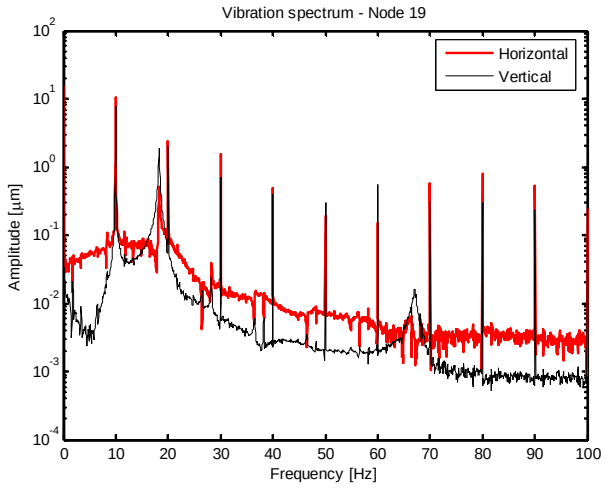


**Figure 26: Vibration spectrum in seal position at 600 rpm.**

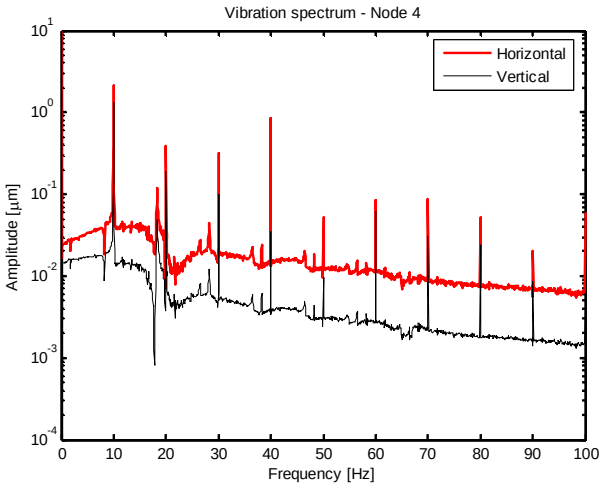


**Figure 27: Vibration spectrum in bearing #1 at 600 rpm.**

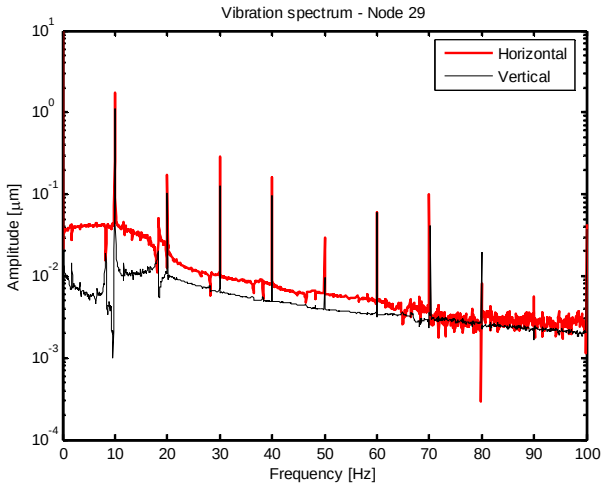


**Figure 28: Vibration spectrum in bearing #2 at 600 rpm.**

## 3.2 Simulation results at 1200 rpm

Also considering the rotating speed of 1200 rpm, thus over the system critical speed, the proposed model is able to reproduce the corresponding experimental behaviour in its main characteristics. Orbit shape, see figure 29 to figure 31 that show 1 s of simulation and the comparison with experimental orbits (rigidly shifted as explained in section 3.1), is pretty well reproduced in all the nodes corresponding to the experimental measuring planes. The contact is intermittent, see figure 32, and its time interval is less than one quarter of the revolution period, similarly to the experimental case shown in figure 17.

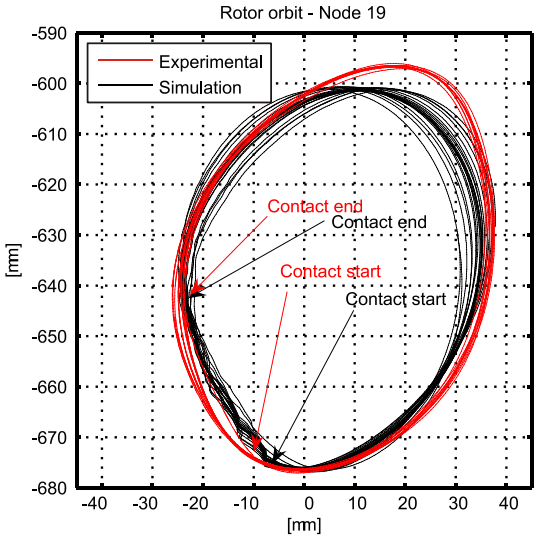


**Figure 29: Rotor orbit in seal position at 1200 rpm.**

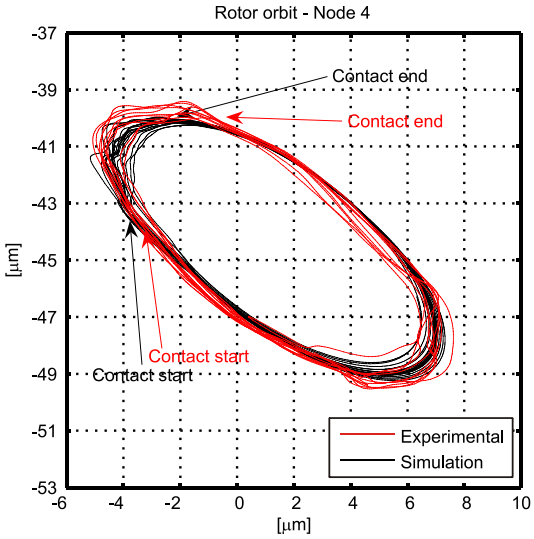


**Figure 30: Rotor orbit in bearing #1 at 1200 rpm.**

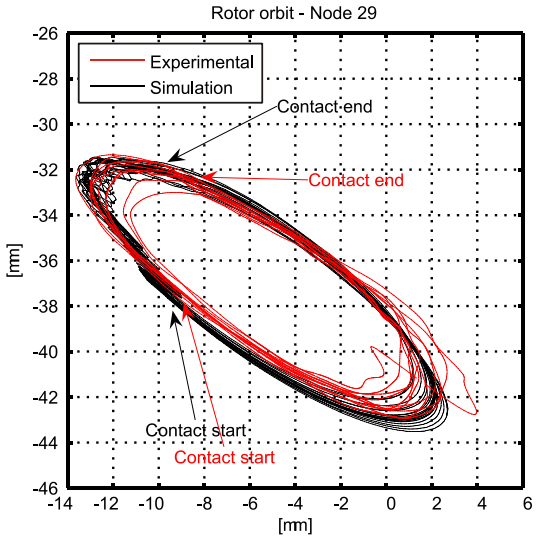


**Figure 31: Rotor orbit in bearing #2 at 1200 rpm.**

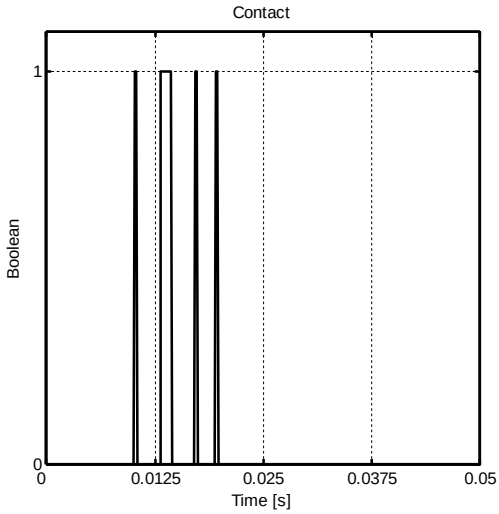


**Figure 32: Time history of the contact over one revolution.**

Vibration spectra in the nodes corresponding to the measuring planes are shown in figure 33-figure 35. The presence of $n\times$ components and their amplitudes correspond to those of the experimental ones in figure 18-figure 20, but also in this case the higher frequency resolution points out them better than in the experimental case. Once again, amplitudes of harmonics are very similar to those of experimental tests.

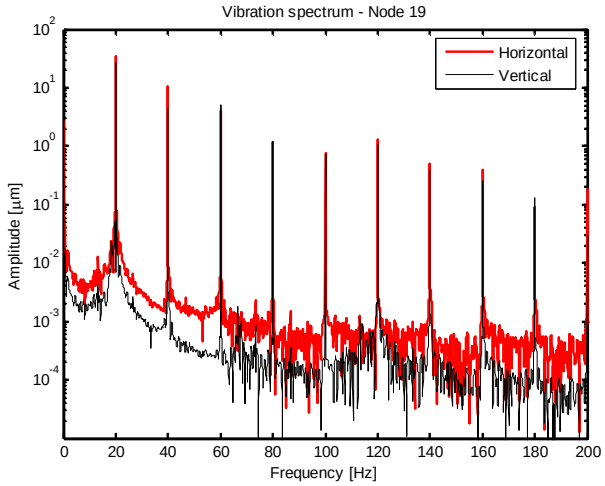


**Figure 33: Vibration spectrum in seal position at 1200 rpm.**

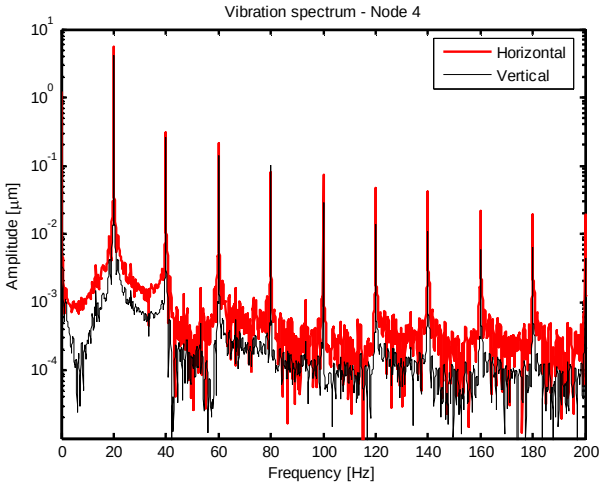


**Figure 34: Vibration spectrum in bearing #1 at 1200 rpm.**

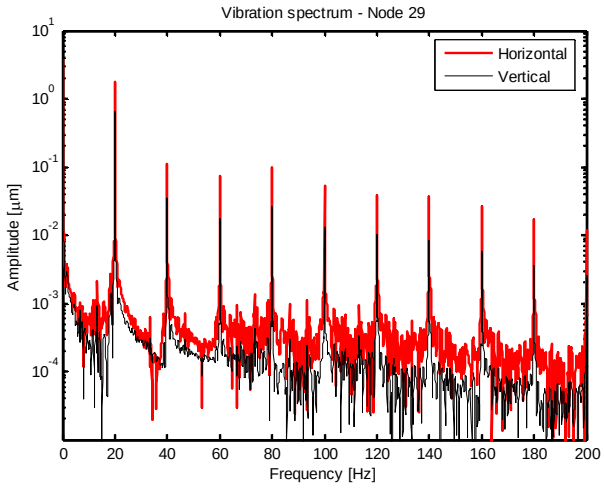


**Figure 35: Vibration spectrum in bearing #2 at 1200 rpm.**

## 4 Conclusions

In this paper, an experimental study and a mathematical model aimed to analyze the effects of rotor to stator rub on seals is presented. A special characteristic of the experimental set-up and of the model is that the fixed part is less stiff than the rotor, reproducing what happens in real systems when the shaft-line interferes with labyrinth seals. The experimental results allowed highlighting the characteristics of the short arc rub, especially with regard to the non-linearities. The model proposed, that uses finite element modelling for the shaft and considers also the degrees of freedom of the seal, allowed reproducing the experimental results obtained on the test rig and can be considered as reliable to simulate also the behaviour of real machines, provided that the rub is light and the seal is relatively soft. The possibility of the model to consider also torsional vibrations, excited by the rub, encourages the use of this model to study also this phenomenon, supplying information that cannot be obtained in real machinery due to the lack of suitable sensors.

## References

[1] Vania, A., Bachschmid, N. and Pennacchi, P., 2001, "Analysis of Light Rotor-to-Stator Contacts in Large Turbine-Generator Units", *Proc. of Surveliance 4 – Acoustical and Vibratory Surveillance Methods and Diagnostic Techniques*, Compiégne, France, October 16-18 2001, pp. 507-516.

[2] Bachschmid N., Pennacchi P., Vania A., Zanetta G.A. and Gregori L., 2004, "Identification of Rub and Unbalance in a 320MW Turbogenerator", *International Journal of Rotating Machinery*, 10(4), pp. 265-281.

[3] Pennacchi P. and Vania A., 2007, "Analysis of Rotor-to-Stator Rub in a Large Steam Turbogenerator," *International Journal of Rotating Machinery*, vol. 2007, Article ID 90631, pp. 1-8.

[4] Curami A., Pizzigoni B. and Vania A., 1986, "On the rubbing phenomena in turbomachinery", Proc. of IFToMM International Conference on Rotordynamics, Tokyo, September 14-17 1986, pp. 481-486.

[5] Stegemann D., Reimche W., Beermann H. and Südmersen U., 1993, "Analysis of Short-Duration Rubbing Process in Steam Turbines", *VGB Kraftwerkstechnik*, 73(10), pp. 739-745.

[6] Hall L.D. and Mba D., 2004, "Diagnosis of continuous rotor–stator rubbing in large scale turbine units using acoustic emissions", *Ultrasonics*, 41(9), pp. 765–773.

[7] Hall L.D. and Mba D., 2004, "Acoustic emissions diagnosis of rotor-stator rubs using the KS statistic", *Mechanical Systems and Signal Processing*, 18(4), pp. 849–868.

[8] Chu F. and Lu W., 2000, "Determination of the rubbing location in a multi-disk rotor system by means of dynamic stiffness identification", *Journal of Sound and Vibration*, 248(2), pp. 235-246.

[9] Peng Z.K., Chu F.L. and Tse P.W., 2005, "Detection of the rubbing-caused impacts for rotor– stator fault diagnosis using reassigned scalogram", *Mechanical Systems and Signal Processing*, 19(2), pp. 391–409

[10] Chu F. and Lu W., 2005, "Experimental observation of nonlinear vibrations in a rub-impact rotor system", *Journal of Sound and Vibration*, 283(3-5), pp. 621–643.

[11] Chu F. and Lu W., 2007, "Stiffening effect of the rotor during the rotor-to-stator rub in a rotating machine", *Journal of Sound and Vibration*, 308(3-5), pp. 758–766.

[12] Fumagalli M. and Schweitzer G. 1996, "Measurements on a rotor contacting its housing, paper c500/085/96, IMechE 6th International Conference on Vibrations in Rotating Machinery, 9-12 September 1996, Oxford, UK pp. 779-788.

[13] Keogh P.S. and Cole M.O.T., 2003, "Rotor vibration with auxiliary bearing contact in magnetic bearing systems. Part 1: synchronous dynamics", *Proc. Instn. Mech. Engrs., Part C: J. Mech. Engr. Sc.*, 217(4), pp. 377-392.

[14] Cole M.O.T. and Keogh P.S., 2003, "Rotor vibration with auxiliary bearing contact in magnetic bearing systems. Part 2: synchronous dynamics", *Proc. Instn. Mech. Engrs., Part C: J. Mech. Engr. Sc.*, 217(4), pp. 393-409.

[15] Choi Y.-S., 2002, "Investigation on the whirling motion of full annular rotor rub", *Journal of Sound and Vibration*, 258(1), pp. 191–198.

[16] Choi Y.-S. and Bae C.-Y., 2001, "Nonlinear dynamic analysis of partial rotor rub with experimental observations", DETC2001/VIB-21634, *Proc. of DETC'01 ASME 2001 Design Engineering Technical Conference and Computers and Information in Engineering Conference*, Pittsburgh, PA, September 9-12, 2001, pp. 1-8.

[17] Choi Y.-S., 2000, "Experimental investigation of partial rotor-rub against a non-rotating part", *Proc. of IMechE-7th Int. Conf. on Vibrations in Rotating Machinery*, Nottingham, UK, 12-14 September 2000, pp. 281-290.

[18] Muszyńska A. and Goldman P., 1995, "Chaotic Responses of Unbalanced Rotor/Bearing/Stator Systems with Looseness or Rubs", *Chaos, Solitons & Fractals*, 5(9), pp. 1683-1704.

[19] Muszyńska A., 2005, "Rotordynamics", CRC Press, Boca Raton, FL, USA.

[20] Hu N.Q. and Wen X.S., 2002, "Chaotic behaviour identification of a rub impact rotor using short term predictability of measured data", *Proc. Instn. Mech. Engrs., Part C: J. Mech. Engr. Sc.*, 216(6), pp. 675-681.

[21] Childs D.W., 1979, "Rub Induced Parametric Excitation in Rotors", *ASME Journal of Mechanical Design*, 101(5), pp. 640-644.

[22] Childs D.W., 1993, "Turbomachinery Rotordynamics", John Wiley & Sons Inc, Chichester, England.

[23] Childs D.W. and Bhattacharya A., 2007, "Prediction of dry-friction whirl and whip between a rotor and a stator", *Journal of Vibration and Acoustics*, 129(3), pp. 355-362.

[24] Bently D.E., Yu J.J. and Goldman P., 2000, "Full Annular Rub in Mechanical Seals, Part I: Experiment Results", *Proc. of ISROMAC-8 Conference*, March 2000, Honolulu, Hawaii, pp. 995-1002.

[25] Bently D.E., Yu J.J. and Goldman P., 2000, "Full Annular Rub in Mechanical Seals, Part II: Analytical Study", *Proc. of ISROMAC-8 Conference*, March 2000, Honolulu, Hawaii, pp. 1003-1010.

[26] Jiang, J. and Ulbrich, H., 2003, "Stability Analysis of Full Annular Rub in Rotor-to-Stator Systems", *PAMM – Proc. Appl. Math. Mech.*, 2(1), pp. 88-89.

[27] Jiang, J. and Ulbrich, H., 2001, "Stability Analysis of Sliding Whirl in a Nonlinear Jeffcott Rotor with Cross-Coupling Stiffness Coefficients", *Nonlinear Dynamics*, 24, pp. 269-283.

[28] Muszynska A., 2002, "Rotor-to-stationary part full annular contact modelling", *ISROMAC-9 Conference*, February 2002, Honolulu, Hawaii, pp. 1-8.

[29] Ehehalt U., Markert R. and Wegener G., 2002, "Stability of Synchronous Forward Whirl at Rotor-Stator-Contact", *ISROMAC-9 Conference*, February 2002, Honolulu, Hawaii, pp. 1-8.

[30] Ehehalt U. and Markert R., 2003, "Instability of Unbalance Excited Synchronous Forward Whirl at Rotor-Stator-Contact", *PAMM – Proc. Appl. Math. Mech.*, 2(1), pp. 60-61.

[31] Ehehalt U. and Markert R., 2003, "Rotor motion during stator contact", Proc. of *6th IFToMM Int. Conference on Rotor Dynamics*, Sydney, pp. 913-920.

[32] Cole M.O.T. and Keogh P.S., 2003, "Asynchronous periodic contact modes for rotor vibration within an annular clearance", *Proc. Instn. Mech. Engrs.* Vol. 217 Part C: J. Mech. Engr. Sc., pp. 1101-1115.

[33] Bachschmid N., Pennacchi P. and Vania A., "Thermally Induced Vibrations due to Rub in Real Rotors", *Journal of Sound and Vibration*, 299(4-5), pp. 683-719.

[34] Edwards S., Lees A.W. and Friswell M.I., 1999, "The influence of torsion on rotor/stator contact in rotating machinery", *Journal of Sound and Vibration*, 225(4), pp. 767-778.

[35] Huang D., 2000, "Experiment on the characteristics of torsional vibration of rotor-to-stator rub in turbomachinery", *Tribology International*, 33(1), pp. 75-79.

[36] Deng X., Liebich R. and Gasch R., 2000, "Coupled bending and torsional vibrations due to rotor-to-stator contacts", *Proc. of IMechE-7th Int. Conf. on Vibrations in Rotating Machinery*, Nottingham, UK, 12-14 September 2000, pp. 291-300.

[37] Bachschmid N., Pennacchi P. and Vania A., 2002, "Identification of Multiple Faults in Rotor Systems", *Journal of Sound and Vibration*, 254(2), pp. 327-366.

[38] Bachschmid N., Tanzi E., Santos M.B., Sexto L.F., 2007, "Some Experimental Results in Rubbing Phenomena Analysis", *Proceedings of Proceedings of the XII International Symposium on Dynamic Problems of Mechanics (DINAME 2007), Ilhabela, SP, Brazil, February 26 - March 2, 2007*, ISBN 978-85-85769-29-1, pp. 1-10.

[39] Pennacchi P., Bachschmid N., Vania A., Zanetta G.A. and L. Gregori, 2006, "Use of Modal Representation for the Supporting Structure in Model Based Fault Identification of Large Rotating Machinery: Part 1 – Theoretical Remarks", *Mechanical Systems and Signal Processing*, 20(3), pp. 662-681.

[40] Lalanne M. and Ferraris G., 1998, "Rotordynamics Prediction in Engineering", John Wiley & Sons Inc, Chichester, England.